Experimental Investigation and Design Optimization of Targeted Energy Transfer Under Periodic Forcing

Etienne Gourc, Guilhem Michon, Sébastien Seguy, Alain Berlioz

Experimental Investigation and Design Optimization of Targeted Energy Transfer under Periodic Forcing

Etienne Gourc

Université de Toulouse

Institut Clément Ader, INSA

F-31077, Toulouse, FRANCE

e-mail: gourc@insa-toulouse.fr

Guilhem Michon

Université de Toulouse

Institut Clément Ader, ISAE

F-31055, Toulouse, FRANCE

e-mail: guilhem.michon@isae.fr

Sébastien Seguy

Université de Toulouse

Institut Clément Ader, INSA

F-31077, Toulouse, FRANCE

e-mail: seguy@insa-toulouse.fr

Alain Berlioz

Université de Toulouse

Institut Clément Ader, UPS

F-31062, Toulouse, FRANCE

e-mail: alain.berlioz@univ-tlse3.fr

ABSTRACT

In this paper, the dynamic response of a harmonically forced Linear Oscillator (LO) strongly coupled to a

Nonlinear Energy Sink (NES) is investigated both theoretically and experimentally. The system studied comprises a LO with an embedded, purely cubic NES. The behavior of the system is analyzed in the vicinity of $1:1$ *resonance. The complexification-averaging technique is used to obtain modulation equations and the associated fixed points. These modulation equations are analyzed using asymptotic expansion to study the regimes related to relaxation oscillation of the slow flow called Strongly Modulated Response (SMR). The zones where SMR occurs are computed using a mapping procedure. The Slow Invariant Manifolds (SIM) is used to derive a proper optimization procedure. It is shown that there is an optimal zone in the forcing amplitude–nonlinear stiffness parameter plane, where SMR occurs without having a high amplitude detached resonance tongue. Two experimental setups are presented. One is not optimized and has a relatively high mass ratio (*$\approx 13\%$*) and the other one is optimized and exhibits strong mass asymmetry (mass ratio* $\approx 1\%$*). Different frequency response curves and associated zones of SMR are obtained for various forcing amplitudes. The reported experimental results confirm the design procedure, and the possible application of NES for vibration mitigation under periodic forcing.*

1 Introduction

Over the past decade, it has been demonstrated that the addition of small mass, with a strong nonlinear attachment to a linear system may give rise, under transient loading, to localization and irreversible transfer of energy, also called pumping. It has been shown that the pumping phenomenon can be explained by studying the nonlinear normal modes of the undamped system [1,2]. More recent studies have introduced a suitable asymptotic procedure based on the invariant manifold approach to include damping force [3]. Addition of a Nonlinear Energy Sink (NES) drastically changes the dynamic response of the whole system, and may be beneficial to vibration mitigation. Energy pumping under transient loading has been widely studied theoretically [4–7] and experimentally [7–9]. More recently, differents configurations of NES and their effect on the damping behavior of a structure have been studied in [10]. In addition to transient loading, systems with NES under periodic forcing have also been studied. Steady state response (response with almost constant amplitude) was studied in [11,12] for a grounded NES. The use of a NES in the field of acoustics has been studied experimentally in [13,14]. The use of a piecewise linear NES has been studied in [15]. The Complexification–Averaging (CX-A) technique [16] has been used to derive modulation equation and compute the fixed points. These regimes have also been analytically and experimentally studied for an embedded NES in [17]. The possibility of using NES in the presence of gravity has been investigated in [18]. It has been demonstrated that in addition to weak quasiperiodic response, which is related to a Hopf bifurcation of the slow flow, systems with NES can exhibit more complex mechanisms for vibration mitigation. These regimes are related to relaxation oscillations and are not related to slow flow fixed points. When the system exhibits the latter type of response (often called Strongly Modulated Response (SMR)), the amplitude of modulation is comparable to the amplitude of the response itself. SMR regimes have been studied in detail in [19,20]. A NES design methodology has been proposed in [21] and the result was compared to numerical simulations.

This paper aims to provide experimental developments of energy pumping under periodic forcing and also a NES design procedure. The next section is devoted to the theoretical treatment of the equation of motion. In the third section, two

different experiments and design procedures are presented. The experimental measurements are compared to theoretical prediction. The last section presents the concluding remarks.

2 Theoretical developments

The theoretical developments presented herein are based on [19, 21]. The system studied in this paper is composed of a harmonically excited Linear Oscillator (LO) strongly coupled to a Nonlinear Energy Sink (NES) (see Fig. 1) and is described by the following equation of motion:

$$m_1\frac{d^2x_1}{dt^2}+c_1\frac{dx_1}{dt}+c_2\left(\frac{dx_1}{dt}-\frac{dx_2}{dt}\right)+k_1x_1+ k_2\left(x_1-x_2\right)^3=k_1x_e+c_1\frac{dx_e}{dt} \tag{1}$$

$$m_2\frac{d^2x_2}{dt^2}+c_2\left(\frac{dx_2}{dt}-\frac{dx_1}{dt}\right)+k_2\left(x_2-x_1\right)^3=0 \tag{2}$$

[Fig. 1 about here.]

Where x_1, m_1, c_1, k_1 and x_2, m_2, c_2, k_2 are the displacement, mass, damping and stiffness of the LO and the NES respectively. All the physical parameters, including the damping of the LO, are taken into account. The imposed harmonic displacement x_e is expressed as follow:

$$x_e=G\cos\tilde{\Omega}t \tag{3}$$

2.1 Fixed points

After rescaling, system (1,2) is reduced to a more convenient form:

$$\ddot{x}_1+\varepsilon\lambda_1\dot{x}_1+\varepsilon\lambda_2\left(\dot{x}_1-\dot{x}_2\right)+x_1+\varepsilon K\left(x_1-x_2\right)^3= \varepsilon F\cos\Omega\tau-\varepsilon^2\lambda_1F\omega\sin\Omega\tau \tag{4}$$

$$\varepsilon\ddot{x}_2 + \varepsilon\lambda_2(\dot{x}_2 - \dot{x}_1) + \varepsilon K(x_2 - x_1)^3 = 0 \tag{5}$$

Where the dots denote differentiation with respect to τ and the following parameters are defined:

$$\{\tau, \omega_1, \omega_2, \varepsilon, \lambda_1, \lambda_1, \Omega, K, F\} =$$
$$\left\{\omega_1 t, \sqrt{\frac{k_1}{m_1}}, \sqrt{\frac{k_2}{m_2}}, \frac{m_2}{m_1}, \frac{c_1}{m_2\omega_1}, \frac{c_2}{m_2\omega_1}, \frac{\tilde{\Omega}}{\omega_1}, \frac{\omega_2^2}{\omega_1^2}, \frac{G}{\varepsilon}\right\}$$

It should be noticed that the rescaled equations are identical for imposed force or displacement up to $O(\varepsilon)$. New variables are introduced as follow:

$$v = x_1 + \varepsilon x_2, \quad w = x_1 - x_2 \tag{6}$$

As the system is studied in the vicinity of the $1:1$ resonance where both oscillators oscillate at the excitation frequency Ω, it is convenient to introduce the following complex variables [16]:

$$\phi_1 e^{i\Omega\tau} = \dot{v} + i\Omega v, \quad \phi_2 e^{i\Omega\tau} = \dot{w} + i\Omega w \tag{7}$$

Introducing Eq. (6,7) into (4,5), and keeping only terms containing $e^{i\Omega\tau}$ yields to the following slow modulated system:

$$\dot{\varphi}_1 + \frac{i\Omega}{2}\varphi_1 + \frac{\varepsilon\lambda_1}{2(1+\varepsilon)}(\varphi_1 + \varepsilon\varphi_2) - \frac{i(\varphi_1 + \varepsilon\varphi_2)}{2\Omega(1+\varepsilon)} - \frac{\varepsilon F}{2} - \frac{i\varepsilon^2\lambda_1 F\Omega}{2} = 0 \tag{8}$$

$$\dot{\varphi}_2 + \frac{i\Omega}{2}\varphi_2 + \frac{\varepsilon\lambda_1}{2(1+\varepsilon)}(\varphi_1 + \varepsilon\varphi_2) - \frac{i(\varphi_1 + \varepsilon\varphi_2)}{2\Omega(1+\varepsilon)} + \frac{\lambda_2(1+\varepsilon)}{2}\varphi_2 - \frac{3iK(1+\varepsilon)}{8\Omega^3}\varphi_2^2|\varphi_2| - \frac{\varepsilon F}{2} - \frac{i\varepsilon^2\lambda_1 F\Omega}{2} = 0 \tag{9}$$

A detuning parameter σ representing the nearness of excitation frequency to the reduced natural frequency of the LO is introduced as follow:

$$\Omega = 1 + \varepsilon\sigma \tag{10}$$

Fixed points of Eq. (8,9) correspond to the periodic solutions of system (4,5). They are computed by equating the derivatives to zero, yielding a system of complex algebraic equations. After algebraic operations, this system is expressed in a more convenient form:

$$\dot{\varphi}_1 = \dot{\varphi}_2 = 0 \Rightarrow \varphi_1(\tau) = \varphi_{10}, \varphi_2(\tau) = \varphi_{20}$$

$$\varphi_{10} = \frac{\dfrac{i\varepsilon\varphi_{20}}{(1+\varepsilon)(1+\varepsilon\sigma)} - \dfrac{\varepsilon^2\lambda_1\varphi_{20}}{1+\varepsilon} + \varepsilon F + i\varepsilon^2\lambda_1 F(1+\varepsilon\sigma)}{i(1+\varepsilon\sigma) + \dfrac{\varepsilon\lambda_1}{1+\varepsilon} - \dfrac{i}{(1+\varepsilon)(1+\varepsilon\sigma)}} \tag{11}$$

$$\alpha_3 Z_{20}^3 + \alpha_2 Z_{20}^2 + \alpha_1 Z_{20} + \alpha_0 = 0, \quad Z_{20} = |\varphi_{20}|^2 \tag{12}$$

Coefficients α_i ($i = 1..3$) are given in Appendix A. To study the stability of these fixed points, small perturbations are introduced:

$$\varphi_1 = \varphi_{10} + \rho_1, \quad \varphi_2 = \varphi_{20} + \rho_2 \tag{13}$$

Keeping only linear terms with respect to ρ_i ($i = 1..2$), taking the complex conjugate and putting the resulting system into matrix form, the stability of the fixed points is then deduced by analyzing the root of the characteristic equation. If a real root crosses the left-half complex plane, it corresponds to a Saddle-Node (SN) bifurcation and if a pair of complex

conjugates crosses the left-half complex plane, it corresponds to a Hopf bifurcation of the slow flow.

2.2 Asymptotic analysis

As the case of small mass ratio ($\varepsilon << 1$) is studied here, Eq. (8,9) are analyzed using a perturbation method. Multiple time scales are introduced as follows:

$$\begin{aligned} &\varphi_i = \varphi_i(\tau_0, \tau_1, \ldots), \quad \frac{d}{d\tau} = \frac{\partial}{\partial \tau_0} + \varepsilon \frac{\partial}{\partial \tau_1} + \ldots, \\ &\tau^k = \varepsilon^k \tau, \quad k = 0, 1, \ldots \end{aligned} \tag{14}$$

Substituting Eq. (10) and (14) into Eq. (8,9) and equating coefficients of like power of ε yields:

$$\begin{aligned} &\varepsilon^0 : \frac{\partial}{\partial \tau_0}\varphi_1 = 0 \\ &\quad \frac{\partial}{\partial \tau_0}\varphi_2 + \frac{\lambda_2}{2}\varphi_2 + \frac{i}{2}(\varphi_2 - \varphi_1) - \frac{3iK}{8}\varphi_2^2|\varphi_2| = 0 \end{aligned} \tag{15}$$

$$\begin{aligned} &\varepsilon^1 : \frac{\partial}{\partial \tau_1}\varphi_1 + \frac{i}{2}(\varphi_1 - \varphi_2) + i\sigma\varphi_1 + \frac{\lambda_1}{2}\varphi_1 - \frac{F}{2} = 0 \\ &\quad \frac{\partial}{\partial \tau_1}\varphi_2 + \frac{i}{2}(\varphi_1 - \varphi_2) + \frac{i\sigma}{2}(\varphi_1 + \varphi_2) + \frac{\lambda_1}{2}\varphi_1 + \frac{\lambda_2}{2}\varphi_2 \\ &\quad - \frac{3iK(1 - 3\sigma)}{8}\varphi_2^2|\varphi_2| - \frac{F}{2} = 0 \end{aligned} \tag{16}$$

The first equation of (15) gives:

$$\frac{\partial \varphi_1}{\partial \tau_0} = 0 \Rightarrow \varphi_1 = \varphi_1(\tau_1, \ldots) \tag{17}$$

Substituting Eq. (17) into the second equation of (15), fixed points $\Phi(\tau_1)$ depend only on time scale τ_1 and obey the following algebraic equation:

$$\frac{\lambda_2}{2}\Phi + \frac{i}{2}\Phi - \frac{i}{2}\varphi_1 - \frac{3iK}{8}\Phi^2|\Phi| = 0 \tag{18}$$

$$\Phi = \lim_{\tau_0 \to \infty} \phi_2$$

Equation (18) is solved by taking $\Phi(\tau_1) = N_2 e^{i\delta_2}$:

$$\begin{aligned} |\phi_1|^2 &= \lambda_2^2 Z_2 + Z_2 - \frac{3K}{2}Z_2^2 + \frac{9K^2}{16}Z_2^3 \\ Z_2(\tau_1) &= N_2(\tau_1)^2 \end{aligned} \tag{19}$$

The number of solutions to Eq. (19) depends only on the parameter λ_2. The roots of the derivative of the right hand side of Eq. (19) are computed to find the critical value of λ_2:

$$Z_{2,i} = \frac{4\left(2 \pm \sqrt{1 - 3\lambda_2^2}\right)}{9K} \qquad i = 1,2 \tag{20}$$

Therefore, if $\lambda_2 < 1/\sqrt{3}$, two roots and a pair of saddle-node bifurcation exist and does not exist otherwise. In fact, Eq. (19) represents the Slow Invariant Manifold (SIM) of the problem. In the case $\lambda_2 > 1/\sqrt{3}$, the SIM is monotonous. On the othe hand, if $\lambda_2 < 1/\sqrt{3}$, the SIM admits extrema and is divided into two stable branches and one unstable branch. An illustration of the SIM is given in Fig. 2 where $K = 100$ and $\lambda_2 = 0.2$. Such a SIM structure may give rise to relaxation oscillations. In effect, the slow flow may rise on the first stable branch until reaching the fold point Z_{21}. The slow flow will jump onto the upper stable branch of the SIM to the landing point Z_{2u}. The amplitude of the slow flow will decrease slowly until reaching the second fold point Z_{22} to jump back to the lower stable branch on point Z_{2d}. To investigate this possibility, the behavior of Eq. (16) on the SIM is analyzed.

[Fig. 2 about here.]

Introducing Eq. (18) into the first equation of (16) yields:

$$\frac{\partial}{\partial\tau_1}\left[2i\left(-\frac{\lambda_2}{2}\Phi-\frac{i}{2}\Phi+\frac{3iK}{8}\Phi^2|\Phi|\right)\right]$$
$$+2i\left(\frac{i}{2}+\sigma i+\frac{\lambda_1}{2}\right)\left(-\frac{\lambda_2}{2}\Phi-\frac{i}{2}\Phi+\frac{3iK}{8}\Phi^2|\Phi|\right)$$
$$-\frac{i}{2}\Phi-\frac{F}{2}=0 \tag{21}$$

By expressing $\Phi(\tau_1)$ in polar coordinates, the equations governing the evolution of N_2 and δ_2 with respect to time scale τ_1 are obtained:

$$\frac{\partial N_2}{\partial\tau_1}=\frac{f_1(N_2,\delta_2)}{g(N_2)} \qquad \frac{\partial\delta_2}{\partial\tau_1}=\frac{f_2(N_2,\delta_2)}{g(N_2)} \tag{22}$$

where

$$f_1(N_2,\delta_2)=-9\lambda_1K^2N_2^5+24\lambda_1KN_2^3-12FKN_2^2\cos\delta_2$$
$$-16\left(\lambda_2+\lambda_1+\lambda_2^2\lambda_1\right)N_2+16F\cos\delta_2+16\lambda_2F\sin\delta_2 \tag{23}$$

$$f_2(N_2,\delta_2)=\left(-54K^2\sigma-27K^2\right)N_2^4+(96K\sigma+12K$$
$$-24\lambda_2\lambda_1K)N_2^2+36KFN_2\sin\delta_2-16\lambda_2^2-32\sigma-32\sigma\lambda_2^2$$
$$+\frac{16\lambda_2F\cos\delta_2-16F\sin\delta_2}{N_2} \tag{24}$$

$$g(N_2)=54K^2N_2^4-96KN_2^2+32+32\lambda_2^2 \tag{25}$$

It has been demonstrated [20] that Eq. (22) admits two types of fixed point. The first type is referred to as ordinary fixed points and is found for $f_1=f_2=0$ and $g\neq0$. These fixed points corresponds to those computed in Eq. (12) if the term at $O(\varepsilon^2)$ is neglected. The others are referred to as folded singularities and are found for $f_1=f_2=g=0$. The system $f_1=f_2=0$ is rewritten in matrix form:

$$\begin{bmatrix} a_{11} & a_{12} \\ a_{21} & a_{22} \end{bmatrix} \begin{pmatrix} \sin\delta_2 \\ \cos\delta_2 \end{pmatrix} = \begin{pmatrix} b_1 \\ b_2 \end{pmatrix} \tag{26}$$

with

$$\begin{aligned} a_{11} &= 16\lambda_2 F, & a_{12} &= -12FKN_2^2 + 16F, \\ a_{21} &= \frac{36FKN_2^2 - 16F}{N2}, & a_{22} &= \frac{16\lambda_2 F}{N_2}, \end{aligned}$$

$$\begin{aligned} b_1 &= 9\lambda_1 K^2 N_2^5 - 24\lambda_1 K N_2^3 + 16N_2\left(\lambda_1 + \lambda_2 + \lambda_2^2\lambda_1\right), \\ b_2 &= \Big[27K^2N_2^5\left(1+2\sigma\right) - 12KN_2^3\left(1 - 2\lambda_1\lambda_2 + 8\sigma\right) \\ &\quad + 16N_2\left(\lambda_2^2 + 2\sigma\lambda_2^2 + 2\sigma\right)\Big]/N_2 \end{aligned} \tag{27}$$

Ordinary fixed points are found by solving Eq. (26) for $\sin\delta_2$ and $\cos\delta_2$, and assuming that the determinant does not vanish. It can be noticed that $\det(a) = 8F^2 g/N_2$, so that, when eliminating f_1 and g, the condition $f_2 = 0$ is automatically satisfied by Eq. (26), thus obtaining the expression of the folded singularities:

$$\begin{aligned} \Delta_{i,j} = \gamma_i \pm \arccos\Big[&N_{2,i}\left(16\lambda_1 - 24\lambda_1 K N_{2,i}^2 + 9\lambda_1 K^2 N_{2,i}^4 + 16\lambda_2\right. \\ &\left. + 16\lambda_1\lambda_2^2\right) / \left(4F\sqrt{9K^2N_{2,i}^4 - 24KN_{2,i}^2 + 16 + 16\lambda_2^2}\right)\Big], \end{aligned} \tag{28}$$

$$\gamma_i = \arcsin\left(\frac{4\lambda_2}{\sqrt{9K^2N_{2,i}^4 - 24KN_{2,i}^2 + 16 + 16\lambda_2^2}}\right)$$

A condition for the excitation amplitude for the existence of folded singularities on the lower and upper fold is obtained

from Eq. (28):

$$\left| \frac{N_{2,i}\left(16\lambda_1 - 24\lambda_1 K N_{2,i}^2 + 9\lambda_1 K^2 N_{2,i}^4 + 16\lambda_2 + 16\lambda_1\lambda_2^2\right)}{4F\sqrt{9K^2N_{2,i}^4 - 24KN_{2,i}^2 + 16 + 16\lambda_2^2}} \right| \leq 1 \tag{29}$$

Yielding:

$$\begin{aligned} F \geq F_{ic} = N_{2,i}\left(16\lambda_1 - 24\lambda_1 K N_{2,i}^2 + 9\lambda_1 K^2 N_{2,i}^4 + 16\lambda_2\right. \\ \left. +16\lambda_1\lambda_2^2\right) / \left(4\sqrt{9K^2N_{2,i}^4 - 24KN_{2,i}^2 + 16 + 16\lambda_2^2}\right) \end{aligned} \tag{30}$$

However, the condition on Eq. (30) is necessary but not sufficient to guarantee the stability of SMR regimes. Under certain conditions, the slow flow may be attracted to another stable response. This mechanism of annihilation of SMR is explained in detail in [22]. To access this possibility, a procedure of 1D mapping has been developed in [20]. The principle consists in following the slow flow during one cycle of relaxation, with initial conditions inside the interval $[\Delta_{11}, \Delta_{12}]$.

The procedure is illustrated in Fig. 3 and consists of four steps described below:

1. A starting point is chosen on the lower fold (see Eq. (20)) with a phase inside the interval $[\Delta_{11}, \Delta_{12}]$. The landing points on the upper fold are then computed using Eq. (18) and the invariant property of the SIM (see Fig. 2 for the corresponding notation):

$$\begin{aligned} -\frac{1}{2}\lambda_2\Phi_{2,1} - \frac{1}{2}i\Phi_{2,1} + \frac{3}{8}iK\Phi_{2,1}^2|\Phi_{2,1}| \\ = -\frac{1}{2}\lambda_2\Phi_{2,u} - \frac{1}{2}i\Phi_{2,u} + \frac{3}{8}iK\Phi_{2,u}^2|\Phi_{2,u}| \end{aligned} \tag{31}$$

2. Equation (22) is numerically integrated with Φ_{2u} as initial conditions, until reaching the upper fold line.
3. The landing point Φ_{2d} on the lower fold is computed in the same way as in the first step.
4. Equation (22) is numerically integrated again, until reaching the lower fold line.

[Fig. 3 about here.]

This procedure is repeated for various starting points inside the interval $[\Delta_{11}, \Delta_{12}]$. Finally, if at the end of step 4, all the points return inside this interval, the SMR cycle is stable. On the other hand, if the slow flow goes through the basin of attraction of a stable fixed point, the SMR cycle is unstable.

3 Experimental tests

In the following section, two different experiments will be presented. The main difference between these experiments is the value of the mass ratio (ε). For the first one $\varepsilon = 12.9\%$ and for the second one $\varepsilon = 1.2\%$. Moreover, the first experiment is subject to harmonic forcing, and the second one to an imposed displacement. As mentioned previously, in the case of base excitation, a term related to the damping of the LO is present (see Eq. (4)); this is not the case for imposed force. However, this term is of $O(\varepsilon^2)$ and does not have that much influence on the behavior of the whole system. In both cases, the displacement is measured using contact–less laser sensors. Raw signals are recorded using a digital oscilloscope and a band pass filter is applied to correct biases and suppress high frequency noise. The cubic stiffness has been implemented geometrically with two linear springs that extend axially and are free to rotate. The force-displacement relationship (given in Eq. (32)), expanded in Taylor series, is shown to be approximately cubic in nature.

$$f = 2k_l u + \frac{2u\left(P - k_l l\right)}{\sqrt{l^2 + u^2}} \approx \frac{2P}{l}u + \frac{k_l - P}{l^3}u^3 + O\left(u^5\right) \tag{32}$$

Where u is the displacement, k_l is the linear spring stiffness, l the initial length of the spring, and P is the pre–stress force. Experimentally, P must be kept as small as possible. Precision rail guides are used for all guidance. For each test, the Root Mean Square (RMS) value of the absolute displacement of the LO (x) and the relative displacement between the NES and the LO (w) are plotted versus the frequency of excitation. RMS values are used in order to highlight the benefits of SMR cycles.

3.1 First experiments with $\varepsilon = 12.9\%$

The first experimental fixture built to investigate the behavior of a single-degree-of-freedom oscillator strongly coupled to a NES under excitation is depicted in Fig. 4. It consists of a main mass (LO) grounded by means of a linear spring, and connected to an electrodynamic shaker. The nonlinear oscillator is embedded on this main mass. Both masses are connected by means of an essential cubic stiffness.

[Fig. 4 about here.]

As shown in Fig. 4, the main system receives the electrodynamic force directly from the modal shaker. This force is constant whatever the response of the system. It has therefore been considered as the input excitation force, and the mass and stiffness of the shaker are considered together with the LO. The exciter force is obtained by measuring the current delivered by the power amplifier. The nonlinear stiffness value used in the theoretical analysis has been obtained with a nonlinear least square cubic polynomial fitting of the experimental curve.

[Table 1 about here.]

The parameters identified on the experimental setup and used for the calculations are given in Tab. 1.

The aim of the experimental tests is to obtain the nonlinear Frequency Response Function (FRF) of the system around the $1:1$ resonance. To this end, the displacement signals of both the LO and the NES have been recorded for increasing and decreasing frequency varying from $5\,Hz$ to $20\,Hz$.

Figure 5 show the nonlinear response curves for the NES and the LO respectively, for a forcing amplitude of $2.7\,N$. Thin lines correspond to stable periodic motion, and thick lines refer to unstable region of periodic solutions. "SN" and "Hopf" indicate the location of the Saddle-Node and Hopf bifurcation points obtained analytically using Eq. (13). In addition to the classical resonance curve, a secondary resonance curve with a stable upper branch is observed.

Those figures also display the measured frequency response of both oscillators, where "o" and "$*$" denote periodic and quasiperiodic regimes respectively, and arrows show the jumps and the direction of evolution of the frequency. For an increasing frequency, the motion takes place on the stable upper branch before jumping onto the lower branch at $12.5\,Hz$. Then, the amplitude of motion increases again when following the main resonance curve. At this time, weak quasiperiodic regime takes place. A time measurement of such a regime is depicted in Fig. 6. This clearly shows a modulated response which match well with a Hopf bifurcation. However, unlike the analytical prediction, motion of the oscillators becomes periodic again before jumping back onto the lower curve. Nevertheless, the frequency at which the jump occurs is approximately the same in both cases.

[Fig. 5 about here.]

[Fig. 6 about here.]

Comparing experimental and theoretical results, it is interesting to notice that there is a qualitative agreement even if differences occur with the amplitude, and instability zones, that are mainly due to the uncertainty in the characterization of the nonlinear stiffness and damping. In this experiment, no SMR has been observed. As it has been shown in [22], in addition to the previously mentioned mechanism of annihilation of SMR, when the mass ratio increases above a given threshold ε_{cr2} (not computed here), neither stable SMR nor unstable limit cycles are possible, and only stable weak modulated response is observed. These considerations motivated the design of a new experiment.

3.2 NES optimization

The previously presented experiment has two major drawbacks:

1. The mass ratio was too high to allow SMR response.
2. A high amplitude detached resonance tongue appeared on the left of the main backbone branch.

In this section, a design procedure is proposed to eliminate this detached resonance tongue and to allow SMR response at the same time, considering a system with a small mass ratio ($\varepsilon \approx 1\%$). To study the conditions for the appearance of the detached resonance tongue, boundaries separating single and triple solutions in Eq. (12), corresponding to Saddle-Node bifurcation, are analyzed. Saddle-Node bifurcation arises when a real root of the characteristic polynomial leaves the left–half complex plane. By setting the root to 0, the resulting equation is written in the following form:

$$v_2 Z_{20}^2 + v_1 Z_{20} + v_0 = 0 \tag{33}$$

Coefficients v_i are not given here due to their length. Eliminating Z_{20} from Eq. (33) yields:

$$Z_{20} = \frac{-v_1 \pm \sqrt{v_1^2 - 4 v_2 v_0}}{2 v_2} \tag{34}$$

Substituting Eq. (34) into Eq. (12) and solving for F produces the boundary separating single from multiple solutions in the plane of parameters (F, σ). An illustration is given in Fig. 7.

[Fig. 7 about here.]

Fig. 7 highlights that there is a narrow zone ($F_{1c} < F < F_{SN}$) where SMR may be possible ($F > F_{1c}$) and where no high amplitude detached resonance tongue exists. This zone is optimal for passive control of vibration using a NES. Taking arbitrary values for ε, λ_1 and λ_2, the boundaries for optimal NES sizing are plotted in the plane of parameters (F, K) in Fig. 8. The nonlinear stiffness K must be chosen inside the interval between the solid and the dashed curve.

[Fig. 8 about here.]

In Figure 9 the evolution of the width of the zone of SMR as a function of the forcing amplitude is presented. It is observed, that this zone is larger when the forcing amplitude is close to the boundary F_{SN}, which is interesting from a vibration mitigation point of view. In the next section the experimental setup designed using the proposed criterion is presented.

[Fig. 9 about here.]

3.3 Second experiments with $\varepsilon = 1.2\%$

The second experiment is depicted in Fig. 10. Here, the whole setup is embedded on a 10 kN elecrodynamic shaker. Feedback position control of the electrodynamic shaker ensures a constant excitation amplitude (especially during SMR regimes).

[Fig. 10 about here.]

The moving masses of the LO and the NES are: $m_1 = 4.178kg$ and $m_{NES} = 0.042kg$ respectively. As the mass of the NES is very small, the inertia of the springs is no longer negligible and has to be considered. In a rough approximation, considering the spring as a beam and neglecting axial inertia, the kinetic energy of the NES is written as follows:

$$T_{NES} = \int_0^{l_0} \rho_S \left(\frac{x}{l_0} \dot{y} \right)^2 dx + \frac{1}{2} m_2 \dot{y}^2 \tag{35}$$

Where $\rho_S = m_S/l_0$ is the mass density of the spring. Thus the moving mass of the NES is $m_2 = 2m_S/3 + m_{NES}$. The natural frequency and the viscous damping factor of the main linear system are estimated by performing modal analysis without the NES. The damping coefficient of the linear guide of the NES has also been estimated by removing the nonlinear stiffness, adding a linear spring and performing modal analysis. The friction in the spring's attachment is neglected. The parameters are summarized in Tab. 2.

[Table 2 about here.]

The nominal excitation amplitude is fixed to define the NES stiffness ($G = 0.25mm$; $F = 0.02$). The sizing curves corresponding to the physical parameters of the system are presented in Fig. 11.

[Fig. 11 about here.]

The red horizontal line corresponds to the dimensionless nominal forcing amplitude, and the two black dots correspond to the excitation amplitude for which the trials have been performed, for the chosen stiffness ($K = 1874$). Both the measured force-displacement relationship and the cubic fitting are presented in Fig. 12 for the designed NES.

[Fig. 12 about here.]

The first results carried out at the nominal forcing amplitude ($G = 0.25mm$) are presented in Fig. 13. The analytical frequency response function is presented in blue, and the experimental one in green. The gray dashed line and the red one represent the theoretical and experimental zone where SMR occurs. The thin black line corresponds to the theoretical FrF of the LO without NES. Theoretically at the resonance frequency, the RMS amplitude of the LO without NES is $x_{RMS} = 0.106$ which is significantly reduced by the NES

[Fig. 13 about here.]

Experimentally, energy pumping through SMR is observed for this forcing amplitude and time response is presented in Fig. 14 corresponding to "Point A" in Fig. 13. It is clear that this regime is related to relaxation oscillation. For this forcing amplitude, no detached resonance curve is observed.

[Fig. 14 about here.]

Fig. 15 shows the obtained frequency response functions for $G = 0.325mm$. Energy pumping still occurs, but high vibration amplitudes before the natural frequency are also observed. This is in accordance with the analytical predictions in Fig. 11. The width of SMR zone is also larger when the excitation amplitude increases, as reported theoretically in Fig. 9.

[Fig. 15 about here.]

The previous results highlight discrepancies between theoretical prediction and experimental measurements in the SMR zone. Numerical simulations have revealed that this zone is sensitive to the damping of both LO and NES, which may explain the difference in its width. It is also observed that, in the both cases, SMR zones shift to the right–hand–side. This is certainly due to a nonlinearity induced in the linear spring anchorage of the LO. However, the behavior observed experimentally shows that energy pumping, under harmonic excitation, is possible without having high amplitude detached resonance tongue. Despite the small mass ratio, the NES induces significant changes in the behavior of the main linear system and the frequency response curve of the LO is flattened. Qualitative behavior of the system is fully explained by the theoretical study.

4 Conclusion

In this paper, the dynamic response of a 2 dof system comprising a harmonically excited Linear Oscillator strongly coupled to a Nonlinear Energy Sink was investigated theoretically and experimentally.

The complexification–averaging thechnique was used to derive modulation equations. The modulation equations were analyzed using asymptotic expansion. The zone of existence of stable strongly modulated response was determined using a mapping procedure.

The first experiment presented was not optimized. This experiment had a relatively high mass ratio ($\varepsilon = 12.9\%$). For this case, the so-called strongly modulated response was not observed, but the obtained frequency response function match fairly well with the theoretical prediction (fixed points computed using the complexification averaging technique). A design procedure was then proposed to optimize the system. The aim of this procedure was to avoid the detached resonance curve and allow SMR response at the same time. The improved experiment with $\varepsilon = 1.2\%$ and the associated measurements were presented. Frequency response functions were plotted for two different excitation amplitudes. At both excitation amplitudes, energy pumping by means of strongly modulated response was observed. A good correlation between theoretical and experimental result was observed.

The experiment also showed that it is possible to avoid the detached resonance curve and still have energy pumping, validating the design methodology.

The use of NES under harmonic excitation is a useful vibration mitigation device due to the lack of preferential linear frequency. However, a proper design procedure must be conducted to avoid spurious high amplitude response.

Appendix A

Coefficients of Eq. (12):

$$\alpha_0 = -(1+\varepsilon)^2\left[\varepsilon^2\lambda_1^2(1+\varepsilon\sigma)^2+1\right]F^2(1+\varepsilon\sigma)^4/\Gamma$$

$$\begin{aligned}\alpha_1 = (1+\varepsilon)^2\Big[&2\lambda_2\lambda_1(1+\varepsilon\sigma)^4+\lambda_2^2\Big(\lambda_1^2(1+\varepsilon\sigma)^2+\\&(1+\varepsilon\sigma)^4+\sigma(\varepsilon\sigma+2)\Big(2(1+\varepsilon\sigma)^2+\varepsilon\sigma^2+2\sigma\Big)\Big)+\\&(1+\varepsilon\sigma)^2\Big(\lambda_1^2(1+\varepsilon\sigma)^2+\sigma^2(\varepsilon\sigma+2)^2\Big)\Big]/\Gamma\end{aligned}$$

$$\begin{aligned}\alpha_2 = -3(1+\varepsilon)^2K\Big[&\lambda_1^2(1+\varepsilon\sigma)^2+\sigma(\varepsilon\sigma+2)\times\\&\Big((1+\varepsilon\sigma)^2+\varepsilon\sigma^2+2\sigma\Big)\Big]/\Big(2\Gamma(1+\varepsilon\sigma)^2\Big)\end{aligned}$$

$$\alpha_3 = \frac{9K^2(1+\varepsilon)^2}{64(1+\varepsilon\sigma)^6}$$

With

$$\Gamma = 4\lambda_1^2(1+\varepsilon\sigma)^2+4\left[(1+\varepsilon\sigma)^2+\varepsilon\sigma^2+2\sigma\right]^2$$

References

[1] Gendelman, O. V., Manevitch, L. I., Vakakis, A. F., and M'Closkey, R., 2001. "Energy pumping in nonlinear mechanical oscillators: Part i—dynamics of the underlying hamiltonian systems". *J. Appl. Mech.,* **68**(1), pp. 34–41.

[2] Vakakis, A. F., and Gendelman, O. V., 2001. "Energy pumping in nonlinear mechanical oscillators: Part ii—resonance capture". *J. Appl. Mech.,* **68**(1), pp. 42–48.

[3] Gendelman, O. V., 2004. "Bifurcations of nonlinear normal modes of linear oscillator with strongly nonlinear damped attachment". *Nonlinear Dyn.,* **37**, pp. 115–128.

[4] Quinn, D. D., Gendelman, O. V., Kerschen, G., Sapsis, T. P., Bergman, L. A., and Vakakis, A. F., 2008. "Efficiency of

targeted energy transfers in coupled nonlinear oscillators associated with 1:1 resonance captures: Part i". *J. Sound Vib.,* **311**(3-5), pp. 1228 – 1248.

[5] Sapsis, T. P., Vakakis, A. F., Gendelman, O. V., Bergman, L. A., Kerschen, G., and Quinn, D. D., 2009. "Efficiency of targeted energy transfers in coupled nonlinear oscillators associated with 1:1 resonance captures: Part ii, analytical study". *J. Sound Vib.,* **325**(1-2), pp. 297 – 320.

[6] Vakakis, A. F., McFarland, D. M., Bergman, L. A., Manevitch, L. I., and Gendelman, O. V., 2004. "Isolated resonance captures and resonance capture cascades leading to single-or multi-mode passive energy pumping in damped coupled oscillators". *J. Vib. Acoust.,* **126**(2), pp. 235–244.

[7] Gourdon, E., Alexander, N. A., Taylor, C. A., Lamarque, C. H., and Pernot, S., 2007. "Nonlinear energy pumping under transient forcing with strongly nonlinear coupling: Theoretical and experimental results". *J. Sound Vib.,* **300**(3-5), pp. 522 – 551.

[8] McFarland, D. M., Bergman, L. A., and Vakakis, A. F., 2005. "Experimental study of non-linear energy pumping occurring at a single fast frequency". *Int. J. Nonlinear Mech.,* **40**(6), pp. 891 – 899.

[9] Kerschen, G., McFarland, D. M., Kowtko, J. J., Lee, Y. S., Bergman, L. A., and Vakakis, A. F., 2007. "Experimental demonstration of transient resonance capture in a system of two coupled oscillators with essential stiffness nonlinearity". *J. Sound Vib.,* **299**(4-5), pp. 822 – 838.

[10] Sapsis, T. P., Quinn, D. D., Vakakis, A. F., and Bergman, L. A., 2012. "Effective stiffening and damping enhancement of structures with strongly nonlinear local attachments". *J. Vib. Acoust.,* **134**(1).

[11] Jiang, X., McFarland, D. M., Bergman, L. A., and Vakakis, A. F., 2003. "Steady state passive nonlinear energy pumping in coupled oscillators: Theoretical and experimental results". *Nonlinear Dyn.,* **33**, pp. 87–102.

[12] Malatkar, P., and Nayfeh, A. H., 2007. "Steady-state dynamics of a linear structure weakly coupled to an essentially nonlinear oscillator". *Nonlinear Dyn.,* **47**, pp. 167–179.

[13] Bellet, R., Cochelin, B., Herzog, P., and Mattei, P. O., 2010. "Experimental study of targeted energy transfer from an acoustic system to a nonlinear membrane absorber". *J. Sound Vib.,* **329**(14), pp. 2768–2791.

[14] Mariani, R., Bellizzi, S., Cochelin, B., Herzog, P., and Mattei, P. O., 2011. "Toward an adjustable nonlinear low frequency acoustic absorber". *J. Sound Vib.,* **330**(22), pp. 5245–5258.

[15] Lamarque, C. H., Gendelman, O. V., Ture Savadkoohi, A., and Etcheverria, E., 2011. "Targeted energy transfer in mechanical systems by means of non-smooth nonlinear energy sink". *Acta mech.,* **221**(1), pp. 175–200.

[16] Manevitch, L. I., 2001. "The description of localized normal modes in a chain of nonlinear coupled oscillators using complex variables". *Nonlinear Dyn.,* **25**, pp. 95–109.

[17] Gourc, E., Michon, G., Seguy, S., and Berlioz, A., 2011. "Experimental investigation and theoretical analysis of a nonlinear energy sink under harmonic forcing". In proceedings of ASME, IDECT.

[18] Ture Savadkoohi, A., Lamarque, C. H., and Dimitrijevic, Z., 2012. "Vibratory energy exchange between a linear and a nonsmooth system in the presence of the gravity". *Nonlinear Dyn.*, pp. 1–11.

[19] Starosvetsky, Y., and Gendelman, O. V., 2008. "Response regimes of linear oscillator coupled to nonlinear energy sink

with harmonic forcing and frequency detuning". *J. Sound Vib.,* **315**(3), pp. 746 – 765.

[20] Starosvetsky, Y., and Gendelman, O. V., 2008. "Strongly modulated response in forced 2dof oscillatory system with essential mass and potential asymmetry". *Physica D,* **237**(13), pp. 1719 – 1733.

[21] Starosvetsky, Y., and Gendelman, O. V., 2008. "Attractors of harmonically forced linear oscillator with attached nonlinear energy sink. ii: Optimization of a nonlinear vibration absorber". *Nonlinear Dyn.,* **51**, pp. 47–57.

[22] Starosvetsky, Y., and Gendelman, O. V., 2010. "Bifurcations of attractors in forced system with nonlinear energy sink: the effect of mass asymmetry". *Nonlinear Dyn.,* **59**(4), pp. 711–731.

List of Tables

List of Figures

Table 1. Parameters of the first experiment

Physical Parameters			
m_1	$0.761\,kg$	m_2	$0.098\,kg$
k_1	$5690\,N/m$	k_2	$1.473 * 10^6\,N/m^3$
c_1	$2.4\,Ns/m$	c_2	$0.1\,Ns/m$
Reduced Parameters			
ε	12.9%	λ_2	0.012
λ_1	0.28	K	$2.01 * 10^3$

Table 2. Parameters of the second experiment

Physical Parameters			
m_1	$4.178kg$	m_2	$0.052kg$
k_1	$1.12*10^4 N/m$	c_1	$3.97Ns/m$
c_2	$0.36Ns/m$		
Reduced Parameters			
ε	1.2%	λ_1	1.45
λ_2	0.13		

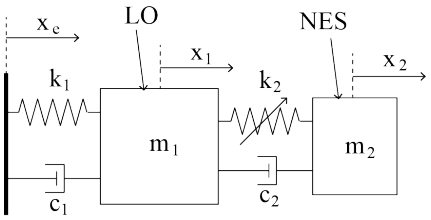

Fig. 1. Schema of the 2 dof system comprising a LO and a NES

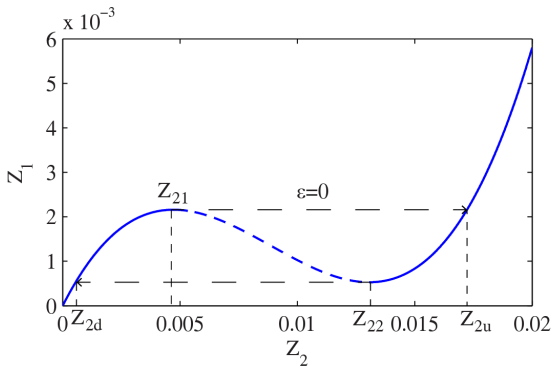

Fig. 2. Exemple of SIM for $K = 100, \lambda_2 = 0.2$

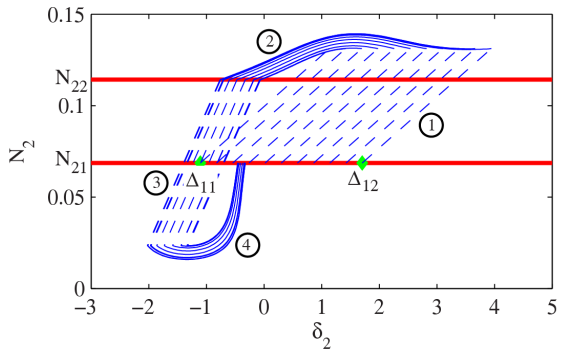

Fig. 3. Illustration of the mapping procedure for $K = 100, \sigma = 1, F = 0.15, \varepsilon = 0.01, \lambda_1 = 0.1, \lambda_2 = 0.2$

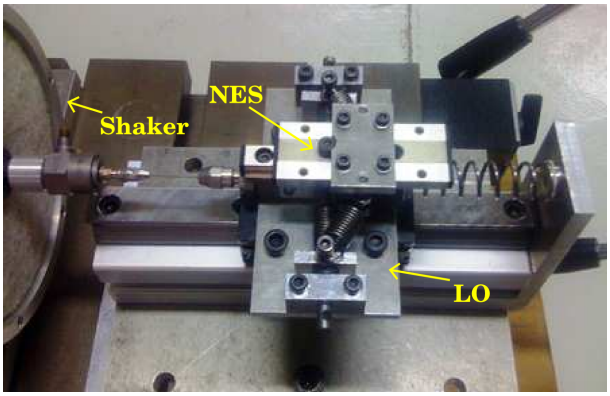

Fig. 4. First experimental set-up ($\varepsilon = 12.9\%$)

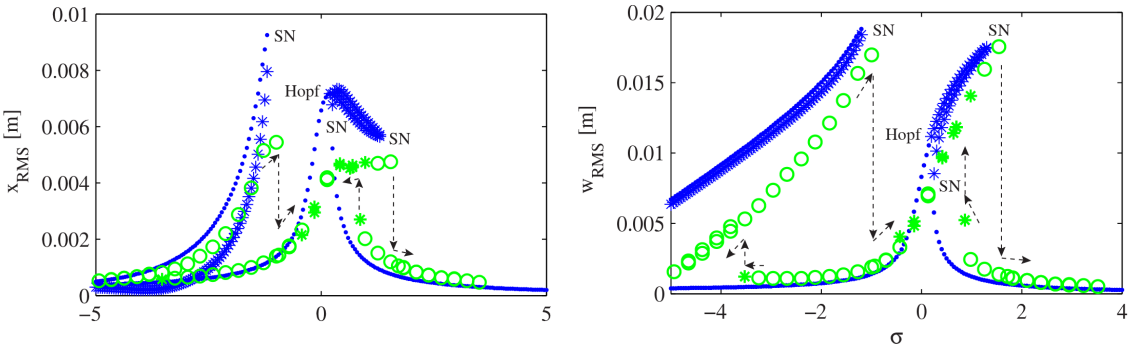

Fig. 5. Experimental (Green) and analytical (Blue) frequency response curve of the LO and the NES for the first experiments and $F = 2.7N$ ("o": experimental periodic oscillation, "$*$": experimental modulated oscillation, thin line: analytical stable fixed points, thick line: analytical unstable fixed point)

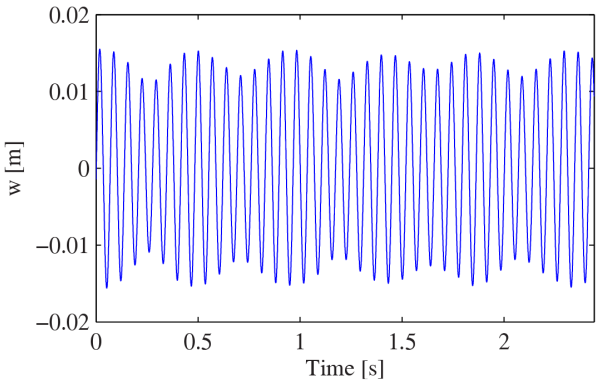

Fig. 6. Experimental measure of weak quasi-periodic response for $F = 2.7N$, $f = 14.5Hz$, $\varepsilon = 12.9\%$

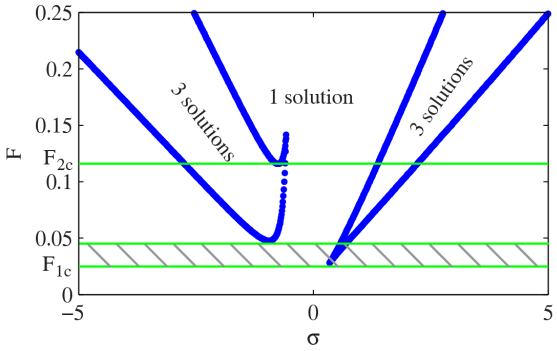

Fig. 7. Boundary of the Saddle-Node bifurcation for $K = 100, \varepsilon = 0.01, \lambda_1 = 0.1, \lambda_2 = 0.2$

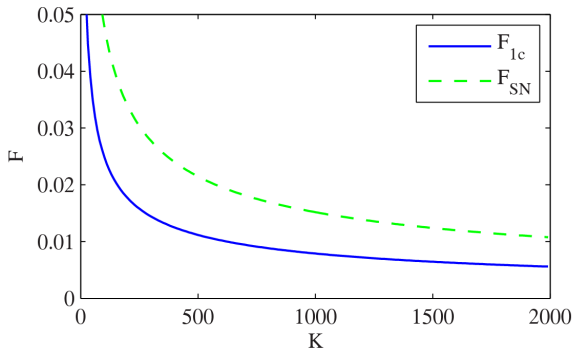

Fig. 8. Critical forcing amplitude as a function of the nonlinear stiffness $\varepsilon = 0.01, \lambda_1 = 0.1, \lambda_2 = 0.2$

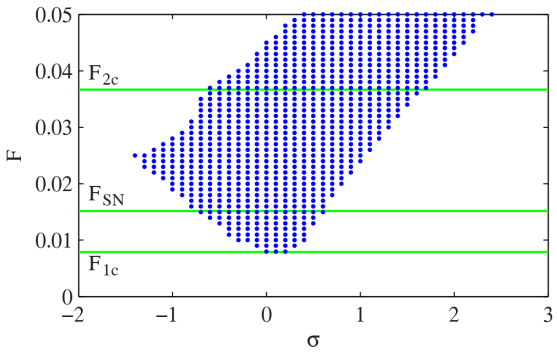

Fig. 9. Zone of SMR as a function of the forcing amplitude for $K = 1000$, $\varepsilon = 0.01$, $\lambda_1 = 0.1$, $\lambda_2 = 0.2$

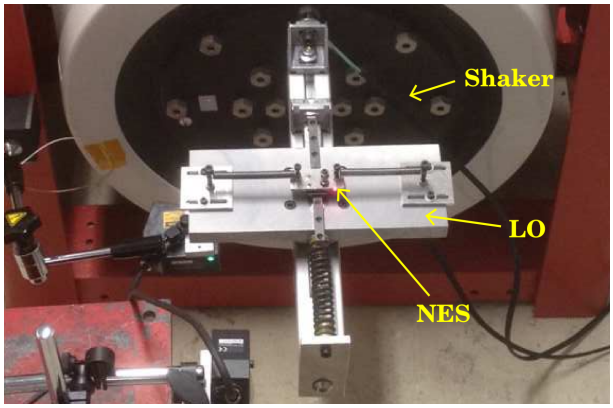

Fig. 10. General view of the second experimental set-up ($\varepsilon = 1.2\%$)

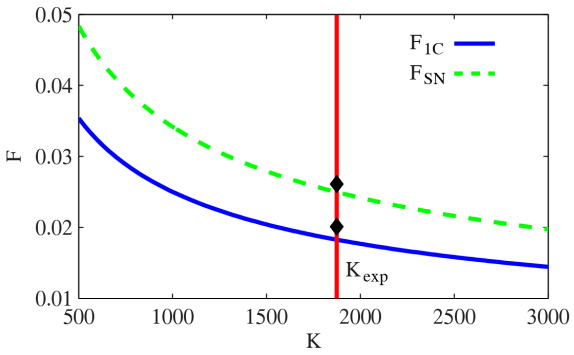

Fig. 11. Design curve corresponding to physical parameters

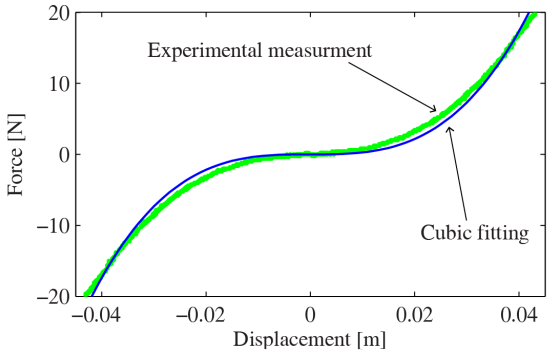

Fig. 12. Force-displacement relationship of the designed NES

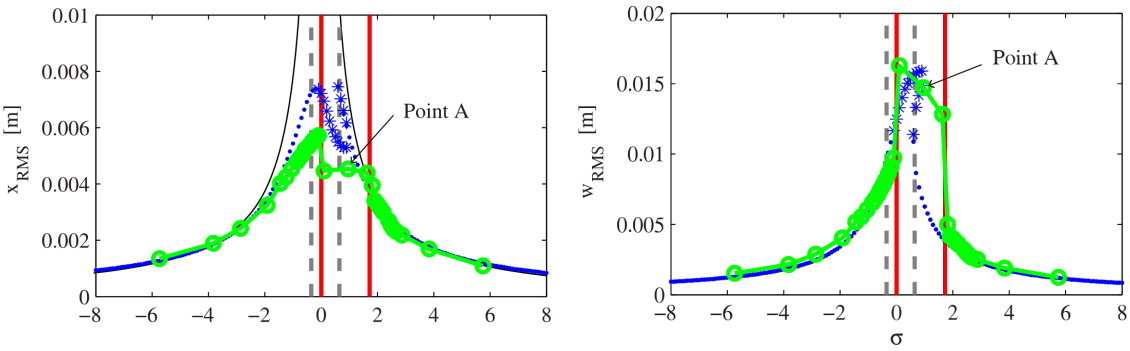

Fig. 13. Experimental (Green) and analytical (Blue) frequency response curve of the LO and the NES for the second experiments and $G = 0.25mm$ (vertical red line : analytically determined zone of SMR, vertical dashed line: experimentally determined zone of SMR, thin black line: theoretical FrF without NES)

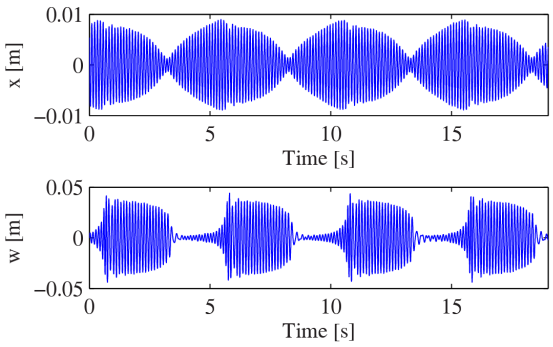

Fig. 14. Experimental measurement of SMR with the second experiment with $G = 0.25mm$, $f = 8.5Hz$, $\varepsilon = 1.2\%$ (Point A in Fig. 13)

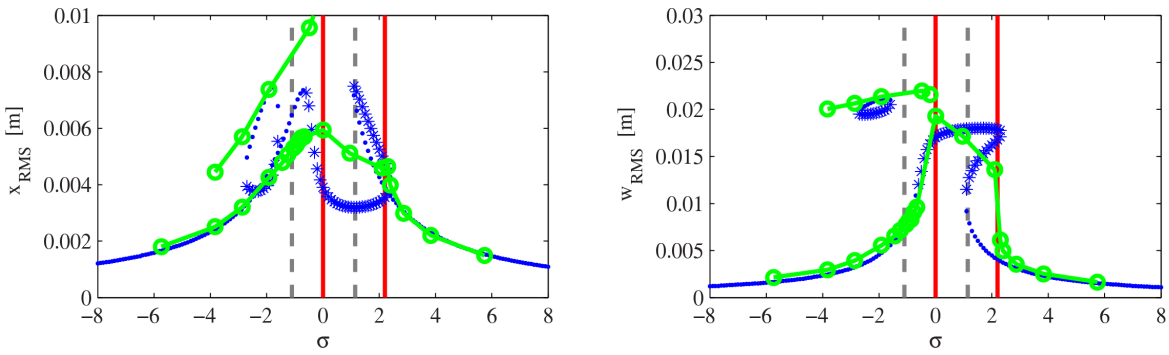

Fig. 15. Experimental (Green) and analytical (Blue) frequency response curve of the LO and the NES for the second experiments and $G = 0.325mm$ (vertical red line : analytically determined zone of SMR, vertical dashed line: experimentally determined zone of SMR)